〔論　　文〕

Effect of the volume of each organ on the dose in computed tomography examination

Osamu KAMEI*, Michihiro ETO*2

School of Health Science Preparatory Office, Nippon Bunri University *
Nippon Bunri University Medical College*2

Abstract

The dose of internal organs during X-ray computed tomography examination can be estimated by Monte Carlo simulation using particle and heavy ion transport system (PHITS) code. However, the direction and dose of the scattered radiation change in a complicated manner depending on the position and size of the organ, affecting the dose. In this study, we investigated body shape factors, such as body weight, effective chest and abdominal diameters, and the volume of each organ, from clinically obtained image data. By conducting multivariate analysis of these data, the body shape factors that affect the dose of each organ were estimated. The results revealed that CED and AED had significant negative regression coefficients for all organs in the body depending on their size. In particular, the effects of heart volume resulted in a negative regression coefficient for all thoracic and abdominal organs, indicating these organs would be affected by the size of the heart.

Keywords: Phantom, Computed tomography (CT), dose, Monte Carlo, multivariate analysis

INTRODUCTION

In recent years, the number of X-ray computer tomography (CT) examinations (hereinafter referred to as CT examinations) has been increasing with the increase in X-ray CT equipment (hereinafter referred to as CT equipment) in Japan(1). In addition, in response to the increase in radiation dose owing to the increase in the number of X-ray examinations, Japan has set a DRL (diagnostic reference level) (2) since June 2015 and the optimized doses for each modality such as CT equipment and IVR (Interventional Radiology) is set.

On 11 March 2019, a partial amendment of the Medical Law Enforcement Regulations stipulated radiation dose management records for patients who undergo X-ray examinations. Furthermore, from 1 April 2020, dose management and recording will be obligatory for each medical institution (3). In the case of CT equipment, there are values, such as CTDIvol (Computed tomography dose index corrected with helical pitch) and DLP (dose length product), as the method of displaying the dose permitted by the enforcement regulations, but they are different from the actual dose of organs because the machine output does not take account of patient geometry.

Meanwhile, organ dose calculation by Monte Carlo simulation (4)(5)(6) is reported to

be the most sophisticated and reliable way to obtain organ doses within bodies of different sizes. CT dose calculators, such as CT-EXPO [7] and ImPACT [8], are typical tools used in clinical settings; these calculators use an algorithm based on normalized dose coefficients derived by Monte Carlo simulation.

In recent years, a dose evaluation method, based on the Monte Carlo simulation method for CT examinations [9][10][11][12], has been developed in conjunction with the development of voxel phantoms [13] and was placed in practical use as an organ dose estimation tool. ImPACT [8] can calculate 27 organ doses by using NRPB-SR250[14] datasets while dividing the human numerical phantoms into 208 5 - mm-thick slices from the head to pelvis. The standard physical size used in these tools to estimate doses is for Caucasians. However, this results presumably in overestimates in smaller Japanese patients.

The Japanese Atomic Energy Agency (JAEA) has developed the JM103 [15] (Japanese male standard body) and JF103 [16] (Japanese female standard body) phantoms as Japanese standard body phantoms. These phantoms are used to estimate organ doses based on Monte Carlo simulations with the PHITS code. The author has investigated and reported on the organ dose evaluation of Japanese adult males and females, based on the use of clinical image data obtained by CT [17]. In the report, it was clarified that there was a strong negative correlation between the physical size and organ dose. In relation to the body's physical size and organ dose, as shown in Figure 1, X-rays emitted from a CT device are generally incident perpendicular to the axis of the body. Among them, it was particularly effective to use effective diameter (ED) (Figure 2) [18] as an index of the physical body size. Under the same source conditions, lean people received higher doses in their internal organs than fat people.

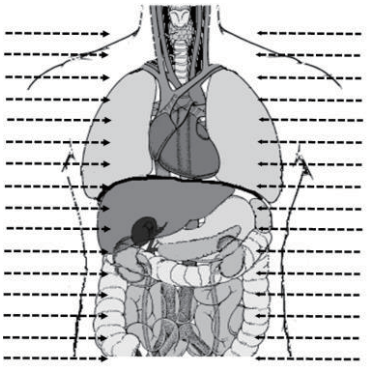

Figure 1 Concept of Organ Scanning during CT Examination

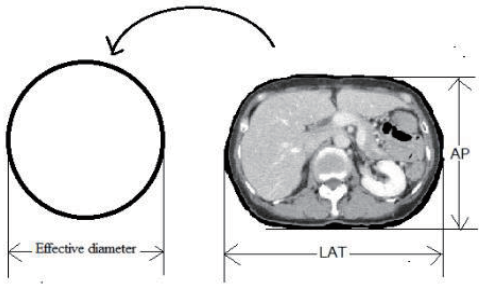

Effective diameter (ED) = $\sqrt{AP \times LAT}$

Figure 2 Calculating effective diameter (ED)

The relationships regarding physical size determined in the present study are consistent with those of Ogden et al. [19]. Turner et al. [20][21] also investigated the eight models of the "GSF family" [22] and found weight and perimeter were well correlated. As described above, ED can be calculated to be equal to the diameter of the perimeter of a circle. Thus, the present results are concordant with those of a previous report [18].

The purpose of this study was to examine the method used to evaluate organ dose during CT examination by analyzing the mechanism of organ exposure during CT examinations by performing multivariate analyses for each numerical value of organ dose and by determining the physical body size, based on simulations.

In an actual CT examination, X-rays are incident vertically on the organ, and at the same time, scattered rays are generated in all directions. Figure 3 shows the scattered rays, according to the PHITS code, when a cylinder of water with a diameter of 20 cm and a length of 20 cm was irradiated with 120 kV X-rays. X-rays were a bundle of lines with a diameter of 2 cm and were irradiated from both sides of the water column with a separation distance of 100 cm from each other. Figure 3a corresponds to the front view in the X-Z direction. Figure 3b also shows a side image in the Y-Z direction and Figure 3c shows a cross-sectional image in the X-Y direction. Therefore, it is clear from the X-ray trajectory that when X-rays are incident on the human body, scattered rays from each organ in the body are scattered in a similar manner along the 360° direction.

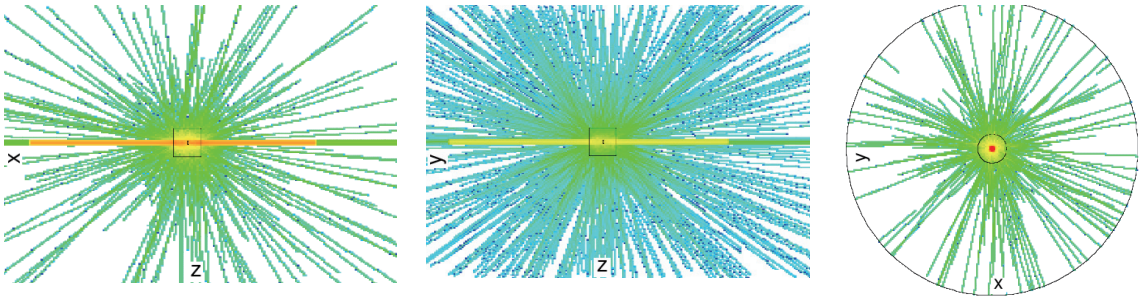

a b c

Figure 3 Occurrence of scattering lines due to interaction between 120kV X-rays and cylinders

Figure 4 shows the results of a simulation assuming changes in scattered radiation, owing to changes in organ density. Figure 4a shows the generation of scattered rays when the cylinder of Figure 3c is surrounded by water with a thickness of 10 cm. Compared with Figure 3c, the scattered radiation is absorbed by the surrounding water and is reduced considerably. In addition, Figure 4b shows the trajectory when water (thickness of 10 cm) is added around it. It can be observed that the scattered radiation is further reduced compared to Figure 4a. Figure 4c shows the trajectory of a simulation in which water outside the cylinder of Figure 4b (thickness: 10 cm) is replaced with human lung tissue (density 0.26 $g \cdot cm^{-3}$).

The presence of less dense organs, such as the lungs, reduces X-ray absorption. As a result, it increases scattered radiation transmission. Therefore, even in each organ in the body, in the case of the heart, it is sandwiched between the left and right lungs in the thoracic cavity, and the dose is affected by the sizes of the lungs. In particular, the upper abdominal organs are considered to be affected by scattered rays from the thoracic cavity. In addition, organs, such as the liver, pancreas, stomach, spleen, and kidneys in the abdominal cavity are in close contact with each other and the scattered radiation generated from each organ is absorbed and scattered, thus affecting the dose of

each organ. Therefore, it is estimated that the dose of each of these organs is affected by the volume of the organ.

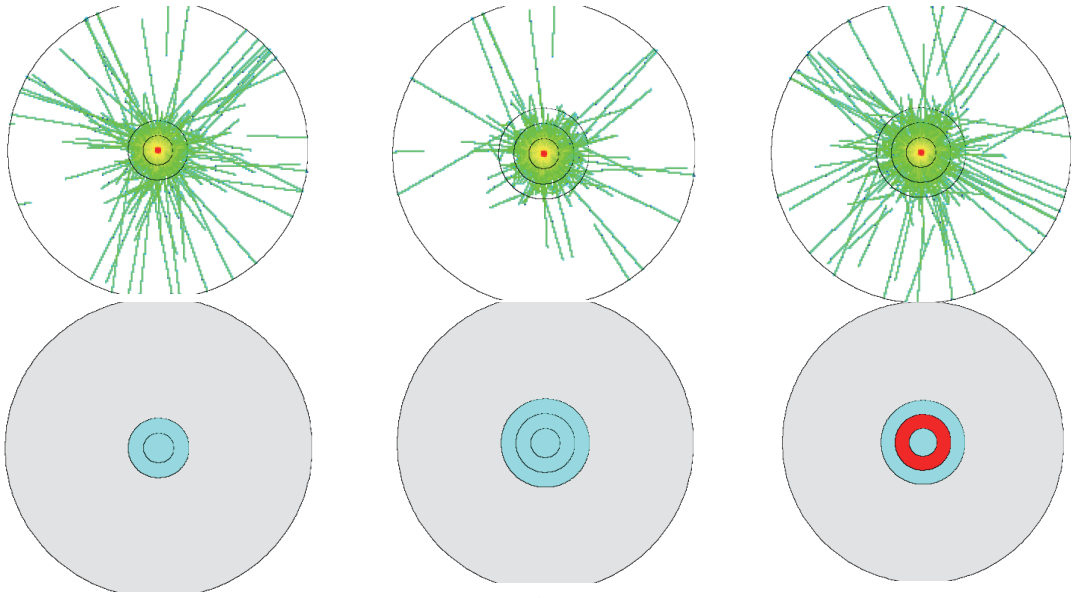

a b c

Figure 4 Changes in X-Y direction scattering lines due to differences in ambient density

By performing multivariate analysis on organ dose data obtained by Monte Carlo simulation as in the present study, the mechanism of exposure during CT examinations is clarified and exposure is reduced. We would also like to validate this analysis method to further improve the accuracy of dose assessment during CT examinations.

MATERIAL AND METHODS

Measurement of body shape from clinical data

From the image data of 11 male patient and 10 female patient who underwent CT examination at the clinical site, height, weight, perimeter, body mass index (BMI), anterior–posterior length (AP), lateral length (LAT) and ED, were all measured.

Those clinical data are provided by Shin-Beppu Hospital (Beppu city Oita Prefecture).

In selecting the sample, rather than random, based on the JM103 and JF103 phantom, was extracted by considering the value of body weight. The patients' weights ranged from 13 kg below that of the JM103 and JF103 phantom to 25 kg above that of the JM phantom. In the human body, AP and LAT differ depending on the position of the chest and abdomen. As a result, the ED also differs. The measurement points for ED were the locations of the pulmonary hilum and central part of the liver.

In addition, the Japanese standard body-type phantom was prepared by JAEA based on the method defined in the 2007 Recommendation [23] of the International Commission on Radiological Protection. The standard phantoms are JM103 (height 172 cm, weight 65 kg) for the male phantom and JF103 (height 155 cm, weight 52 kg) for the female phantom.

Simulation of organ dose

Referring to a commercial X-ray CT device was constructed according to PHITS code [24], and X-rays were irradiated by simulation to estimate the organ dose. In the CT system, the Monte Carlo calculation used the source model of the CT scanner explicitly. The three-dimensional geometry is shown in Fig. 5, which includes the bow-tie filter and collimator. The parameters of this model were as follows: focus–isocenter distance, 57 cm; fan beam angle, 60°; beam width at the isocenter section, 20 mm; focus-collimator distance, 10 cm. The lead collimator material was 2 mm thick and 140 cm long.

The commercial spectrum generation program SPEC78 (Institute of Physics and Engineering in Medicine) [25] was used to create x-ray spectra. The X-ray generation conditions were created, given that the target substance was tungsten, the target angle was 12°, the tube voltage was 120 kV, the voltage pulsation rate was 0%, and the additional filter (5 mm Al) achieved a total filtration of 6.13 mm Al. The X-ray spectrum is shown in Figure 6.

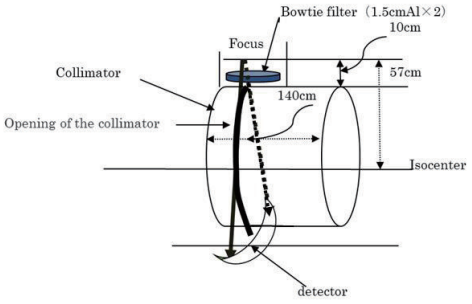

Figure 5 Building an X-ray CT for Simulation

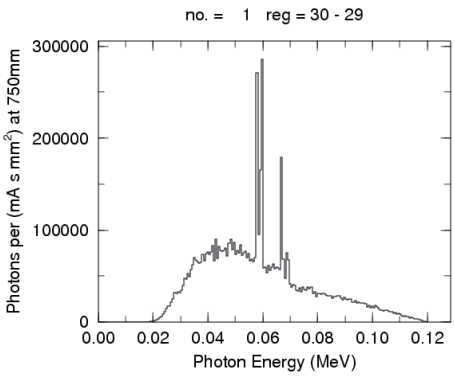

Figure 6 X-ray Spectrum

Voxel conversion of the CT images

A voxel model was created for each patient from his CT image using voxel conversion software. The CT images were created by the CT scans SOMATOM Definition Flash (Siemens Medical Solutions, Forcheim, Germany) and Aquilion 16 (Canon Medical Systems, Inc., Otawara-shi, Japan). Organs (i.e., the liver, stomach, heart, lung, kidneys, spleen, pancreas, gallbladder, and bladder) were segmented.

The voxel model was transformed into the txt data format (500×500). The program for voxel phantom creation was originally developed for this study.

The voxel phantom indicated one voxel of 1 mm^3 in the case of a matrix, 500×500. Each organ volume can be evaluated by calculating the exact number of voxels included in the organ. The simulation of the organ dose was based on the total dose per organ for ~30 scans with a slice width of 20 mm from the upper edge of the chest to the lower end of the pelvis. It was standardized per 1 mAs irradiation of pseudo-X-rays. In addition, the density of each organ in the clinical data used in

this study was simulated as 1.4 g/cm^3 for all skeletons, 1.04 g/cm^3 for each organ except lungs and 0.296 g/cm^3 for the lungs. In addition, the proportions of elements composing each organ were made same.

Statistical processing

In this study, organ doses were estimated via a Monte Carlo simulation using voxel phantoms created from clinical images. Then, a multivariate analysis of organ doses was performed using the ED of the chest and abdomen and organ volumes as indices. Thus, regression equations were obtained for each organ dose and each effective diameter (AED and CDE), and each organ volume as variables.

In multivariate analysis, we first analyzed the multicollinearity of the explanatory variables and examined their combinations. In addition, we analyzed the relationship between the chest ED (CED) and the abdominal ED (AED), and the relationship between body weight and CED and AED, which are considered to be strongly correlated with respect to the body shape. We also analyzed the relationship between body weight and the volume of each organ.

From the obtained simulation results, the dose of each organ in the lung, heart, and abdominal cavity organs was analyzed by multivariate analysis of the volume of each organ and the dose of each organ with the use of JMP (version 12.0: the JMP software is provided by SAS.).

In the multivariate analysis, the response variables were the lung, heart, liver, gallbladder, stomach, pancreas, kidney, and spleen organ doses. In addition, the following numerical values were used as explanatory variables: Weight, CED, AED and volume of each organ, including the sizes of the lung, heart, liver, gallbladder, stomach, pancreas, kidney, and spleen.

RESULTS

Body shape measurement results of clinical data

JM103 and JF103, as well as body mass measurements, height, weight, chest and abdominal APs, and LAT, were measured from clinical images of 11 males and 10 females. ED are listed in Tables 1 (males) and Tables 2 (females).

The standard male phantom is the JM103 phantom, and ① to ⑪ are clinical data numbers. C-AP, C-LAT, and C-Perimeter are the chest region, and A-AP, A-LAT, and A-Perimeter are the abdominal region. The standard female phantom is the JF103 phantom, and ① to ⑩ are clinical data numbers. C-AP, C-LAT, and C-Perimeter are the chest region, and A-AP, A-LAT, and A-Perimeter are the abdominal region.

Table 1 Results of each measurement of male data in the chest and abdomen (cm)

	JM103	①	②	③	④	⑤	⑥	⑦	⑧	⑨	⑩	⑪
Height	171	172	163	170	158	174	160	170	172	172	163	170
Weight (kg)	65	55	55	60	64	66	67	75	78	90	64	80
BMI	22.2	18.5	20.7	20.7	25.6	21.7	26.2	25.9	26.3	30.4	24.1	27.7
C-AP	22.1	20.2	20.1	20.6	22.1	21.3	23.3	26.2	23.9	26.0	23.0	23.0
C-LAT	33.3	29.8	32.8	32.3	32.8	33.5	32.2	36.1	35.8	34.9	31.4	34.9
C-Perimeter	93.7	81	86.8	86.9	89.5	87.6	89.9	101	96.3	98.5	90	93.7
CED	27.1	24.5	25.7	25.8	26.9	26.7	27.4	30.8	29.3	30.1	26.9	28.3
A-AP	21.5	18.1	20.8	20.0	22.3	21.2	25.5	26.8	25.0	26.2	22.8	25.6
A-LAT	30.7	25.3	31.2	31.2	30.3	30.4	32.1	33.2	34.0	34.2	31.0	33.0
A-Perimeter	83.8	70.2	84.8	84.4	84.9	82.6	91.6	97.5	96.5	97.7	89.3	92.9
AED	25.7	21.4	25.5	25.0	26.0	25.4	28.6	29.8	29.2	29.9	26.6	29.1

Table 2 Results of each measurement of female data in the chest and abdomen (cm)

	JF103	①	②	③	④	⑤	⑥	⑦	⑧	⑨	⑩
Height	155	155	155	155	155	158	162	166	152	152	170
Weight (kg)	52	39	70	70	56	51	51	54	74	75	53
BMI	21.6	16.2	29.1	29.1	23.3	20.4	19.4	19.6	32.0	32.5	18.3
C-AP	22.0	18.5	24.2	23.9	21.2	20.9	19.9	18.8	26.3	27.1	18.1
C-LAT	29.9	24.0	34.0	35.6	31.6	32.7	31.3	31.9	33.0	37.4	30.3
C-Perimeter	91.1	71.1	94.3	98.9	86.7	88.5	87.0	84.2	96.4	107	79.8
CED	25.7	21.1	28.7	29.2	25.9	26.1	25.0	24.5	29.5	31.8	23.4
A-AP	18.7	15.3	25.5	25.3	20.8	20.1	18.3	19.3	26.4	27.9	17.8
A-LAT	25.2	24.5	32.8	32.6	30.2	29.0	30.0	27.0	33.9	33.0	26.6
A-Perimeter	73.4	66.3	93.5	96.2	82.9	84.4	81.6	76.7	96.0	98.6	72.8
AED	21.8	19.7	28.9	29.1	25.0	24.1	23.4	22.8	29.9	30.3	21.8

The volumes of JM103 and JF103, as well as internal organs (lung, heart, liver, gallbladder, stomach, pancreas, kidney and spleen) measured from the clinical images of 11 male and 10 female, are listed in Tables 3 (males) and Tables 4 (females).

Table 3 Measurement result of volume of each organ in male data (cm^3)

	JM103	①	②	③	④	⑤	⑥	⑦	⑧	⑨	⑩	⑪
Lung	5,240	4,894	4,838	5,032	3,839	5,480	4,291	4,858	4,848	5,058	3,382	2,441
Heart	896	755	823	752	728	659	758	1,013	1,085	937	1,132	718
Liver	1,240	1,487	1,513	1,423	1,584	1,380	1,086	1,343	1,529	1,887	1,110	1,530
Gallbladder	16	22	20	10	39	19	55	26	10	32	34	19
Stomach	118	175	158	65	223	183	172	122	221	191	127	123
Pancreas	113	98	57	40	89	64	78	58	99	79	59	41
Kidney	252	343	351	333	310	320	323	306	313	306	260	369
Spleen	132	142	199	128	109	144	109	71	200	121	130	237

Table 4 Measurement results of the volume of each organ in female data (cm^3)

	JF103	①	②	③	④	⑤	⑥	⑦	⑧	⑨	⑩
Lung	4,932	3,567	3,470	2,981	3,720	3,595	5,106	3,570	4,119	3,636	3,602
Heart	725	612	664	708	785.2	726	825	854	705	719	799
Liver	1,123	1,141	1,249	1,058	1,255	1,012	1,241	963	1,136	2,373	1,111
Gallbladder	6.7	2.0	29.0	39.8	29.2	16.0	18.0	11.0	29.0	34.0	11.0
Stomach	119.4	45	105	130	141.8	51	146	133	150	151	100
Pancreas	106.8	26	15.2	42.7	50.5	38	50	37	58	62	40
Kidney	237.8	258	283.4	344	305	277	251	243	339	487	242
Spleen	61.6	42	85.5	141.7	81.1	44	91	130	157	298	83

Organ dose simulation results

Subsequently, the estimated results of the dose based on the simulations of internal organs (the lung, heart, liver, gallbladder, stomach, pancreas, kidney and spleen) measured from the clinical images are shows in Figure 7.

Figure 7a shows the results of regression analysis of CED and the doses of the lungs and heart. Figure 7b shows the results of regression analysis of the ED AED of the abdomen and the dose of each organ in the abdomen.

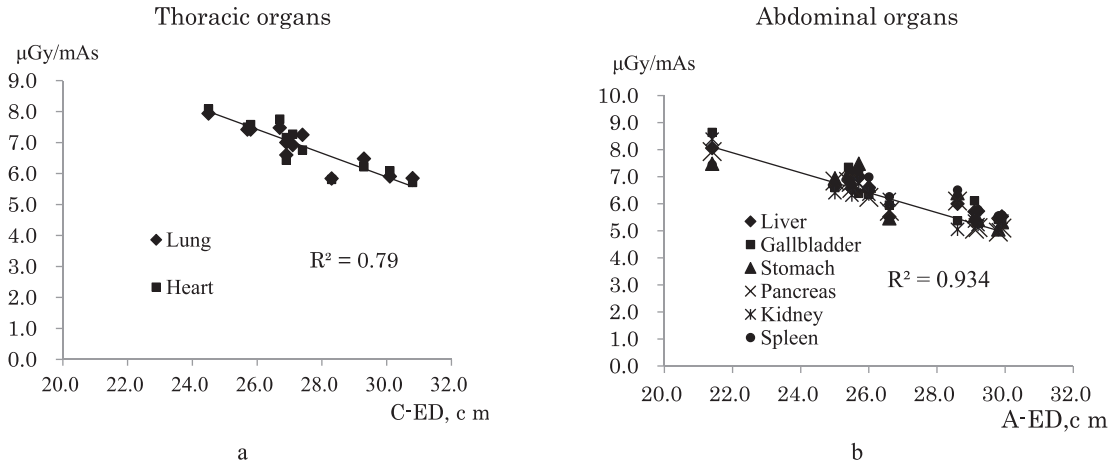

Figure 7 Regression Analysis of Effective Diameter and Organ Dose

Regression analysis of body shape

The correlation between CED and AED in the body type was analyzed.

Subsequently, the correlation between body weight ("Weight") and CED and AED was analyzed.

As a result, the correlation CED and AED is shown in Figures 8a.

Also, the correlation between body weight ("Weight") and CED and AED are shown in Figures 8b and 8c.

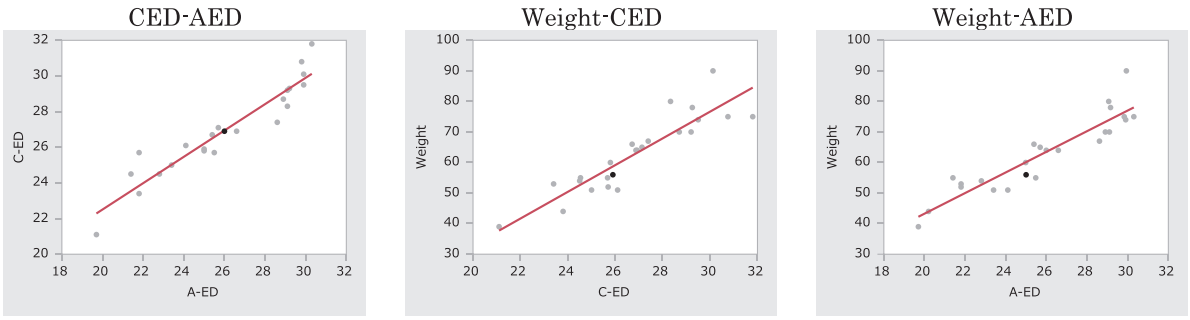

R^2=0.89 P<0.0001 R^2=0.81 P<0.0001 R^2=0.85 P<0.0001

a **b** **c**

Figure 8 Correlation between CED, AED, and Weight

The correlation between body weight ("Weight") and lung and heart volume (size) is shown in Figures 9a and 9b.

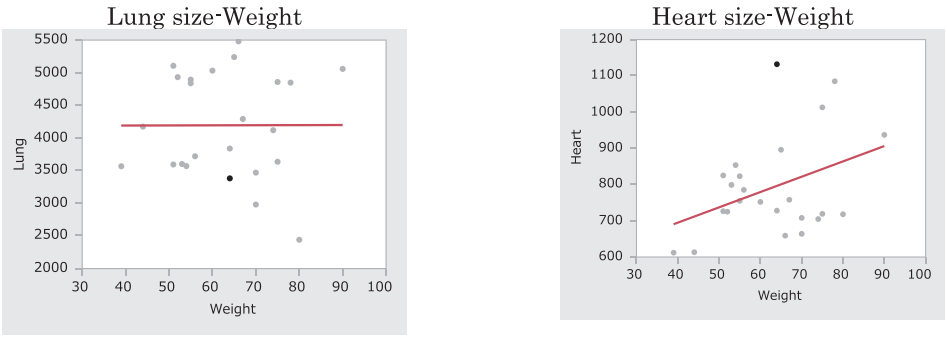

R^2=0.0000058 P=0.99 R^2=0.15 P=0.066

a **b**

Figure 9 Correlation between body weight ("Weight") and volume (size) of organs in the chest

The results of regression analysis of body weight ("Weight") and volume (size) of liver, stomach, pancreas, gallbladder, kidney and spleen are shown in Figures 10a–10f. There was no correlation in the pancreas, but a weak correlation was found in all other organs.

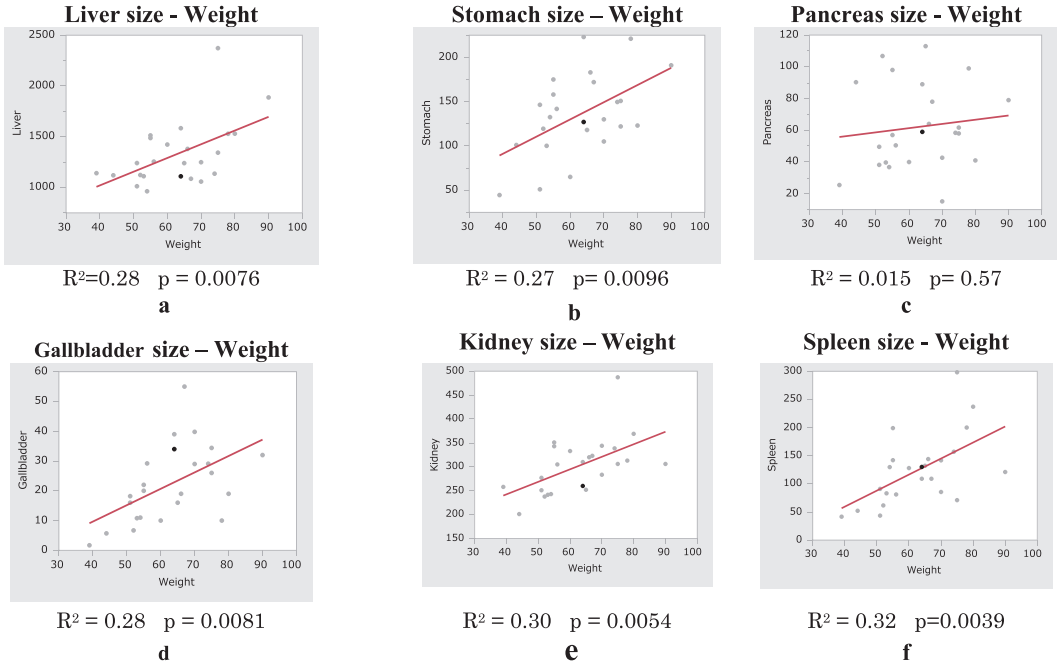

Figure 10 Regression analysis of body weight("Weight") and abdominal organ volume (size)

Multivariate analysis results of organ dose

From the obtained simulation results, the dose of each organ in the lung, heart was analyzed by multivariate analysis of the volume of each organ and the dose of each organ with the use of JMP. Table 5 shows the results of multiple regression analysis of lungs and heart.

Table 5 Multiple regression analysis of organ dose at the lungs and heart organ volume.
R-C: Regression Coefficients

Item		Lung		Heart	
		R-C	p	R-C	p
Constant	a	14.99	<.0001	15.31	<.0001
CED	b	-0.26	0.0006	-0.27	<.0001
Lung	c	0.00015	0.35	0.00026	0.055
Heart	d	-0.0012	0.20	-0.0019	0.012
Liver	e	-0.00051	0.24	-0.00024	0.47
Gallbladder	f	-0.0032	0.79	-0.0079	0.40
Stomach	g	0.0023	0.50	0.00047	0.86
Pancreas	h	-0.0014	0.81	0.0015	0.75

From the obtained simulation results, the dose of each abdominal cavity organs was analyzed by multivariate analysis of the volume of each organ and the dose of each organ with the use of JMP. Tables 6 show the results of multiple regression analysis of each organ in the abdomen.

Table 6 Multiple regression analysis of organ dose at the abdominal organ volume.

R-C: Regression Coefficients

Item		Liver		Stomach		Pancreas		Gallbladder		Kidney		Spleen	
		R-C	p	R- C	p	R- C	p	R- C	p	R- C	p	R-C	p
Constant	a	16.11	<.0001	17.37	<.0001	16.80	<.0001	16.85	<.0001	17.07	<.0001	15.89	<.0001
AED	b	-0.25	<.0001	-0.24	0.0030	-0.31	<.0001	-0.33	0.0001	-0.13	<.0001	-0.20	0.0037
Lung	c	-0.000076	0.62	0.00013	0.55	0.00011	0.54	0.000088	0.67	-0.00015	0.24	-0.000095	0.63
Heart	d	-0.0020	0.042	-0.0036	0.016	-0.0017	0.11	-0.0016	0.22	-0.0011	0.16	-0.0025	0.048
Liver	e	-0.0000049	0.99	-0.00024	0.74	-0.00029	0.61	0.00007	0.92	0.00030	0.48	0.00033	0.62
Gallbladder	f	-0.011	0.39	0.00030	0.99	0.0024	0.87	-0.0032	0.86	-0.0096	0.38	0.0014	0.93
Stomach	g	0.0024	0.46	-0.0024	0.61	-0.0015	0.67	0.0043	0.35	0.00071	0.79	-0.0041	0.34
Pancreas	h	0.00058	0.90	0.0071	0.34	0.0034	0.55	-0.0073	0.30	0.0027	0.53	0.012	0.078
Kidney	i	-0.0034	0.47	-0.0074	0.28	-0.0029	0.58	-0.0031	0.62	-0.0036	0.36	-0.0057	0.35
Spleen	j	0.00049	0.89	0.0036	0.47	0.00044	0.91	0.0028	0.55	-0.00092	0.74	-0.00081	0.85

DISCUSSION

In this study, organ doses were estimated using Monte Carlo simulation using voxel phantoms created from clinical images. Then, a multivariate analysis of organ doses was performed using the ED of the chest and abdomen and organ volumes as indices. Therefore, regression equations were obtained for each organ dose and each effective diameter (AED and CDE), and each organ volume as variables. The results revealed that CED and AED had significant negative regression coefficients for all organs in the body depending on their size.

The estimated results of the dose based on internal organ (the lung, heart, liver, gallbladder, stomach, pancreas, kidney, and spleen) simulations measured from clinical images are shown in Figure 7. The results indicate that the organ dose in all regions linearly decreased with CED (Figure 7a) and AED (Figure 7b).

Regression lines were in good agreement between CED and the lung and heart (Figure 7a) and between AED and internal organs (the liver, gallbladder, stomach, pancreas, kidney, and spleen) (Figure 7b). Correlation analysis between body weight and CED and AED yielded the following results.

Figure 8a shows a strong correlation ($R^2 = 0.89$) between CED and AED in terms of body shape correlation. In addition, Figures 8b and 8c show a strong correlation between body weight and CED ($R^2 = 0.81$) and AED ($R^2 = 0.85$). Therefore, body weight, CED, and AED were not included as explanatory variables simultaneously to avoid multicollinearity in multivariate regression analysis.

Dose analysis of the thoracic organs (lung and heart) was performed using CED only, whereas that of the abdominal organs (liver, stomach, gallbladder, spleen, and kidneys) was performed using AED only.

As a result, as shown in Figures 9a and 9b, CED was not correlated with the lung and heart volumes of the chest organs. Moreover, AED was weakly correlated with the volumes of the abdominal organs (liver, stomach, gallbladder, spleen, and kidneys) but not with the volume of the pancreas. Therefore, multiple regression analysis was performed by assuming no multicollinearity between CED and AED and organ volumes.

Table 5 shows the results of multiple regression analysis of the lung and heart doses, which can be calculated using the following expression (1). This expression shows that the lung and heart volume and CED and each organ volume can predict patient-specific organ doses, where Y(i) is the estimated organ dose using the CED(i) in patient i, a is a constant item, and b to h are regression coefficients of each organ volume.

$$Y(i) = a + b \cdot CED + c \cdot Lung + d \cdot Heart + e \cdot Liver + f \cdot Gallbladder + g \cdot Stomach + h \cdot Pancreas \quad (1)$$

Using the results of multiple regression analysis of lung and heart doses (Table 5), the regression coefficient (b) of CED was −0.26 (p = 0.0006) for the lung and −0.27 (p = 0.0037) for the heart. This can be attributed to the fact that direct X-rays from the CT device were attenuated by the shielding effect of the CED value. The regression coefficient (c) associated with the lung size was 0.00026 (p = 0.055) and was a positive coefficient of cardiac dose, indicating that as the lung volume increases, X-ray absorption decreases, and the heart dose increases.

The regression coefficient (d) of the heart volume was negative (−0.0019; p = 0.012), indicating a self-shielding effect based on the heart volume. Moreover, regression coefficients (e to h) for all abdominal organ volumes were not at the 5% significant level.

Table 6 shows the results of multiple regression analyses of the internal organ doses in the abdomen. This multiple regression analysis revealed that all abdominal organs have negative AED regression coefficients. Similar to the chest, direct X-rays from CT devices have a shielding effect based on the AED value. In addition, the regression coefficient of the heart volume was negative in all organs, indicating that X-rays transmitted through the lungs were blocked by the heart. Thus, each abdominal organ can be calculated using the following expression (2). This expression shows that the lungs and heart and AED and the volume of each abdominal organ can predict patient-specific organ doses.

$$Y(i) = a + b \cdot AED + c \cdot Lung + d \cdot Heart + e \cdot Liver + f \cdot Gallbladder + g \cdot Stomach + h \cdot Pancreas + i \cdot Kidny + j \cdot Spleen \quad (2)$$

where Y(i) is the estimated organ dose using the AED(i) in patient i, a is a constant item, and b to j are regression coefficients of each organ volume.

As a result of multiple regression analysis, the regression coefficient of the heart volume was negative for all abdominal organ doses, indicating that X-rays transmitted through the lungs were blocked by the heart. Among them, regression coefficients (c) for heart volumes were at the 5% significant level for the liver (−0.0020; p = 0.042), stomach (−0.0036; p = 0.016), and spleen (−0.0025; p = 0.048) dose.

Thus, the heart, being close to the liver, is considered to be greatly affected by the shielding effect, and the gallbladder, being adjacent to the stomach and pancreas, is affected by scattered rays from the stomach. The gastric dose was a result that depended on the shielding effects of the heart volume. In addition, the pancreatic dose was

considered to be a positive coefficient with a lung volume and regression coefficient, resulting in a large contribution to scattered radiation and a large shielding effect attributed to the liver volume.

Furthermore, regression coefficients of the lung and liver volumes positively or negatively changed depending on the organ. This positive or negative value is considered to be due to the addition of exposure, owing to scattered radiation from surrounding organs and the absorption of scattered radiation attributed to the shielding effect of surrounding organs, depending on the organ's position.

However, regression coefficients (e to j) for all abdominal organ volumes were not at the 5% significant level.

CONCLUSIONS

Increased radiation dose in our country due to the increasing number of CT examinations has become an important issue in the current healthcare setting. Reducing the radiation dose during CT examinations requires technical innovations in the CT device by the manufacturer. Thus, the exposure mechanism should be considered during CT examinations. Organ exposure during CT examinations has been considered to be only from direct X-rays from the X-ray tube; however, an analysis revealed that in addition to the direct rays, the organs were also exposed to scattered rays generated by each surrounding organ. In particular, the effects of heart volume resulted in a negative regression coefficient for all thoracic and abdominal organs, indicating these organs would be affected by the size of the heart.

REFERENCES

(1) Ono K, Yoshitake T, Hasegawa T, Ban N, Kai M. Estimation of the number of CT procedures based on nationwide survey in Japan. Health Phys 100: 491-496;2011.

(2) Setting the diagnostic reference level based on the latest domestic survey: Japan Network for Research and Information on MedicalExposure: J-RIME,2017.

(3) Ministry of Health, Labour and Welfare: Ministerial Ordinance to partially revise the Ordinance for Enforcement of the Medical Care Act (Ordinance No. 21 of the Ministry of Health, Labour and Welfare),2019.

(4) J. J. DeMarco, C. H. Cagnon, D. D. Cody, D. M. Stevens, C. H. McCollough, J. O'Daniel, and M. F. McNitt-Gray, "A Monte Carlo based method to estimate radiation dose from multidetector CT(MDCT): Cylindrical and anthropomorphic phantoms," Phys. Med. Biol. 50, 3989– 4004 (2005).

(5) J. J. DeMarco, C. H. Cagnon, D. D. Cody, D. M. Stevens, C. H. McCollough, M. Zankl, E. Angel, and M. F. McNitt-Gray, "Estimating radiation doses from multidetector CT using Monte Carlo simulations: Effects of different size voxelized patient models on magnitudes of organ and effective dose," Phys. Med. Biol. 52, 2583–2597 (2007).

(6) J. J. DeMarco, T. D. Solberg, and J. B. Smathers, "A CT-based Monte Carlo simulation tool for dosimetry planning and analysis," Med. Phys. 25, 1–11 (1998).

(7) Stamm, G. and Nagel, H. D. CT-Expo— a novel program for dose evaluation in CT. Rofo. 174, 1570–1576 (2002).

(8) ImPACT. Available on: http://www.impactscan.org/ ctditables.htm.

(9) Jones D G, Shrimpton P C. Survey of CT practice in UL –Part III Normalized organ doses calculated using Monte Carlo techniques-, NRPB-R250, National Radiological Protection Board (NRPB),1991.

(10) Waters L, MCNPX version 2.5.C, Los Alamos National Laboratory Report No. LA-UR-03-2202,2003.

(11) Takahashi F, Endo A, Sato K, Hasegawa T, Katsunuma Y, Ono K, Yoshitake T, Ban N, Kai M. Analysis of organ doses from computed tomography (CT) examination by the radiation transport calculation to develop the dosimetry system, WAZA-ARI. Prog Nucl Sci Technol 1: 517-520; 2011a.

(12) Takahashi F, Endo A, Sato K, Ono K, Yoshitake T, Hasegawa T, Katsunuma Y, Ban N, Kai M, Effects of human model configuration in Monte Carlo calculations on organ doses from CT examinations. Prog Nucl Sci Technol 2: 153-159;2011b.

(13) Fujii K, Aoyama T, Yamauchi-Kawaura C, Koyama S, Yamauchi M, Ko S, Akahane K, Nishizawa K. Radiation dose evaluation in 64-slice CT examinations with adult and paediatric anthropomorphic phantoms. *Br J Radiol.* 82 1010-1018,2009.

(14) D. G. Jones, P. C. Shrimpton, Survey of CT practice in UL –Part III Normalized organ doses calculated using Monte Carlo techniques-, NRPB-R250, National Radiological Protection Board (NRPB) (1991).

(15) Sato K, Noguchi H, Emoto Y, Koga S, Saito K. Japanese adult male voxel phantom constructed on the basis of CT images. *Radiat Prot Dosim.* 123 337-334,2007.

(16) Sato K, Noguchi H, Emoto Y, Koga S, Saito K. Development of a Japanese adult female voxel phantom, *J Nucl Sci Technol.* 46 907-913,2009.

(17) Kamei, O; Ojima, M; Yoshitake, T; Kai, M. Calculating patient-specific organ doses from adult body CT scans by Monte Carlo analysis using male-individual voxel phantoms. *Health Phys.*108(1), 44-52,2015.

(18) American Association of Physicists in Medicine, Size-Specific Dose Estimates (SSDE) in Pediatric and Adult Body CT Examinations AAPM Report No. 204 New York,2011.

(19) Ogden K, Huda W, Scalzetti EM, Roskopf ML. Patient size and x-ray transmission in body CT. Health Phys 86:397-405; 2004.

(20) A. C. Turner, D. Zhang, H. J. Kim, J. J. DeMarco, C. H. Cagnon, E. Angel, D. D. Cody, D. M. Stevens, A. N. Primak, C. H. McCollough, and M. F. McNitt-Gray, "A method to generate equivalent energy spectra and filtration models based on measurement for multidetector CT Monte Carlo dosimetry simulations," Med. Phys. 36(6), 2154–2164 (2009).

(21) A. C. Turner, M. Zankl, J. J. DeMarco, C. H. Cagnon, D. Zhang, E. A. Angel, D. D. Cody, D. M. Stevens, C. H. McCollough, and M. F. McNitt- Gray, "The feasibility of patient size-corrected, scanner-independent organ dose estimates for abdominal CT exams" Med. Phys. 38(2), 820–829 (2011).

(22) Petoussi - Henss, Zanki M, Fill U, Requlla D, The GSF family of voxel phantoms. Phys Med Biol. 2002 Jan 7;47(1):89-106.

(23) International Commission on Radiological Protection. The recommendations of the International Commission on Radiological Protection. Ann ICRP 37(2-4); Publication 103,2007.

(24) Iwase H, Niita K, Nakamura T, "Development of general purpose particle and heavy ion transport Monte Carlo code. *J Nucl Sci Technol.* 39, 1142,2002.

(25) Cranley K, Gilmore B, Fogarty G, and Desponds L, Catalogue of diagnostic x-ray spectra and other data, IPEM Report No. 78,1997.

(2022年12月20日受理)